






## Avalanche properties in striplike ferromagnetic systems

Svetislav Mijatović <sup>\*</sup>, Milica Branković , Stefan Graovac , and Djordje Spasojević   
*Faculty of Physics, University of Belgrade, P. O. Box 44, 11001 Belgrade, Serbia*

 (Received 25 April 2020; accepted 24 July 2020; published 17 August 2020)

We present numerical findings on the behavior of the athermal nonequilibrium random-field Ising model of spins at the thin striplike  $L_1 \times L_2 \times L_3$  cubic lattices with  $L_1 < L_2 < L_3$ . Changing of system sizes highly influences the evolution and shape of avalanches. The smallest avalanches [classified as three-dimension- (3D) like] are unaffected by the system boundaries, the larger are sandwiched between the top and bottom system faces so are 2D-like, while the largest are extended over the system lateral cross section and propagate along the length  $L_3$  like in 1D systems. Such a structure of avalanches causes double power-law distributions of their size, duration, and energy with larger effective critical exponent corresponding to 3D-like and smaller to 2D-like avalanches. The distributions scale with thickness  $L_1$  and are collapsible following the proposed scaling predictions which, together with the distributions' shape, might be important for analysis of the Barkhausen noise experimental data for striplike samples. Finally, the impact of system size on external field that triggers the largest avalanche for a given disorder is presented and discussed.

DOI: [10.1103/PhysRevE.102.022124](https://doi.org/10.1103/PhysRevE.102.022124)

### I. INTRODUCTION

During the past two decades, the study of thin systems has become widely attractive. Having wide industrial and practical implementations, thin systems became an inevitable aspect of everyday life. One important class of such systems are ferromagnetic striplike systems. Thin ferromagnetic systems have been extensively experimentally studied throughout several decades [1–9] which recently led to a number of numerical and theoretical results [10–18].

The essence of the behavior of thin ferromagnetic systems is an avalanche-like relaxation following their externally caused disturbances. More generally, the avalanche-like response of the externally driven systems turned out to be a widespread mechanism in nature. Phenomena such as neuronal activities in the brain [19,20], earthquakes [21], the response of the mechanically pressured wooden materials [22], financial booms and busts [23], as well as the already-mentioned behavior of ferromagnetic materials all have in common that the underlying systems evolve through the metastable states due to avalanche-like relaxation. Such relaxation can eventually lead to extreme events such as huge avalanches that almost span the whole system indicating phase transition in the thermodynamic limit [24].

Within a set of models developed for theoretical and numerical investigation of the avalanche-like behavior [11,25–31], one of the most prominent and most considered remains to be the random-field Ising model (RFIM) [32–34]. So far, both the equilibrium and nonequilibrium versions of the RFIM were intensively theoretically and numerically studied [35–37].

A particular focus of the RFIM studies was the development of the renormalization group approach for description of the RFIM criticality, which turned out to be a rather difficult

task. Perturbative approach gave incorrect predictions in three dimensions [38–40], while the nonperturbative methods led to better results [41,42]. Some recent progress offered important answers on the universality principles [43], dimensional reduction [44], and supersymmetry [45] in the equilibrium model.

Along with the theoretical results, a significant number of numerical studies appeared regarding the critical behavior of RFIM for dimensions  $D \geq 3$  [46–48], the scaling laws of the avalanche parameters [49–51], the critical behavior for  $D = 2$  [52,53]. Recently, the question of the behavior of the systems with changing geometry [54] emerged, together with the reconsideration of the universality classes within the RFIM [55,56].

Among two RFIM versions, the nonequilibrium model appeared to be more relevant for the real experiments because its local type dynamics is closer in describing what happens inside the externally driven ferromagnets. Since in most of experiments the thermal fluctuations are small, here we study the athermal nonequilibrium model.

The paper is organized as follows. An introduction to the model, together with simulation details, are given in Sec. II. Section III presents different types of avalanches in the system and the effective critical disorder is calculated for various system sizes. The behavior of distributions of avalanche size, duration, and energy is presented in Sec. IV and their collapses in Sec. V. In Sec. VI we study how the value of external field for which the susceptibility of the system reaches its maximum changes with system dimensions. In Sec. VII we compare our findings with the past experimental results and finally give a conclusion in Sec. VIII.

### II. MODEL AND SIMULATION DETAILS

The random-field Ising model describes  $N$  ferromagnetically coupled classical spins  $S_i = \pm 1$  in a homogeneous

<sup>\*</sup>corresponding author: [svemij@ff.bg.ac.rs](mailto:svemij@ff.bg.ac.rs)

external magnetic field  $H$  and a random magnetic field  $\{h_i\}_{i=1}^N$  acting at the sites  $i$  of the underlying lattice. The random-field local values  $h$  are chosen from a probability distribution  $\rho(h)$ , here the Gaussian distribution  $\rho(h) = \frac{1}{R\sqrt{2\pi}} \exp(-\frac{h^2}{2R^2})$ , following: (1) at each lattice site  $\langle h_i \rangle = 0$  and  $\langle h_i^2 \rangle = R^2$ , while (2) the values  $h_i$  and  $h_j$  at different sites  $i$  and  $j$  are not correlated,  $\langle h_i h_j \rangle = 0$ ; here  $\langle \dots \rangle$  denotes averaging over all random-field configurations, and  $R$  is the distribution's standard deviation named *disorder*. Random field in this model plays the role of impurities and irregularities in the real ferromagnetic systems. The greater the  $R$ , the greater are those irregularities, which justifies the name assigned to  $R$ . In the athermal version of the model, studied in this paper, the random field is quenched (i.e., frozen in time) which is appropriate for the ferromagnetic systems far below the critical temperature.

In the short-range version of the model all spins are ferromagnetically coupled only with their nearest neighbors so the Hamiltonian of the model reads

$$\mathcal{H} = -J \sum_{\langle i,j \rangle} S_i S_j - H \sum_i S_i - \sum_i h_i S_i, \quad (1)$$

where in the first term the summation  $\sum_{\langle i,j \rangle}$  goes over all distinct pairs of nearest neighbors and  $J$  is their coupling constant, while the remaining two terms describe the coupling of spins with the external field  $H$  and the local value  $h_i$  of the random field at the spin's site.

The foregoing RFIM spin system is driven by the external field that varies in time and in the nonequilibrium RFIM version its evolution is governed by the following local dynamical rule: If at the moment  $t$  of (discrete) time  $t$  the sign of spin  $S_i$  differs from the sign of the effective field  $h_i^{\text{eff}} = J \sum_{\langle j \rangle} S_j + H + h_i$  at its site, then the spin is unstable and will change its sign (i.e., flip) at the next moment of time  $t + 1$ . The flipping of unstable spins may destabilize their neighbors causing them to flip in the next next moment of time, and so on, in which case an avalanche of spin flipping is created lasting until all spins become stable at the current value of  $H$ . In this paper we have studied the adiabatic evolution in which  $H$  remains constant during avalanches that is appropriate for the slowly driven systems with a fast response to the changes of  $H$ . Total number of spins that are flipped during one avalanche represents the avalanche size  $S$  and the time interval between the first and the last flipped spin in that avalanche represents the avalanche duration  $T$ . Another important avalanche parameter is its energy, defined as  $E = \sum_{t=1}^T S_t^2$ , where  $S_t$  is the number of flipped spins in moment  $t$  of an avalanche propagation and  $T$  is the above-mentioned avalanche duration.

In this paper we study the RFIM systems at the striplike  $L_1 \times L_2 \times L_3$  cubic lattices, with  $L_1 < L_2 < L_3$  (see Fig. 1), using closed boundary conditions along length  $L_3$  and open along thickness  $L_1$  and width  $L_2$ . All spins are initially set to  $S_i = -1$  and the external field to  $H = -\infty$ . Thereupon, and after each avalanche,  $H$  is increased so as to flip exactly the least stable spin until reaching the final state with all  $S_i = +1$ . We have chosen the foregoing type of distribution of random fields, as well as the initial and driving conditions, because they were used in the majority of past studies of the nonequilibrium athermal RFIM. Therefore, we consider

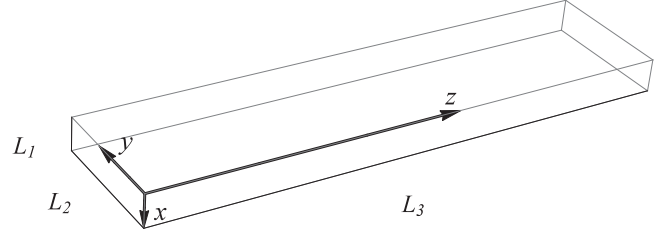


FIG. 1. Striplike system of type  $L_1 \times L_2 \times L_3$ . The  $xyz$  coordinate system is introduced for easier further reference.

them as a natural choice in the initial phase of research of the current topic, leaving the studies under different conditions for the future. The number of spins per one system ranges from  $16 \times 10^3$  to  $17 \times 10^6$ , while the disorders for each system size take values from  $R = 0.1$  to  $R = 2.5$ . The number of different random-field configurations for each system size ranges from 200 for the biggest to 30 000 for the smallest.

In order to minimize the simulation runtime we have encoded in Fortran90 the sorted list algorithm [46,57]. This algorithm efficiently finds the next most unstable spin once the previous avalanche is over. Basically, all values, taken by the random field in the current simulation, are sorted from the largest to the smallest in one list in the beginning and when avalanche ends the algorithm searches for the most unstable spin among the list of spins that would have been most unstable if they had zero flipped, one flipped, or two flipped nearest neighbors. In this way the simulation time per single run was greatly reduced which enabled large number of runs necessary to collect reliable statistics. The simulations are done on a Supermicro server 8047R-7RTF and one runtime for the largest system and largest disorder was about 3 h. The subsequent data analysis was performed with the aid of proprietary programs encoded in Fortran90, Visual Basic, and Wolfram Mathematica.

### III. AVALANCHE FORM AND EVOLUTION

#### A. Effective critical disorder

As mentioned in the previous section, the studied RFIM systems evolve throughout the avalanches of spin flipping. The propagation of avalanches is pinned at the avalanche traps, i.e., lattice sites having large value of random field that prevents the spin at the site to flip until the external field grows enough. If disorder  $R$  is large, then there are many such spins so we do not expect large avalanches to appear. As we decrease  $R$ , bigger and bigger avalanches appear until at (and below) some value of  $R$  the largest avalanches span the whole system along at least one of its dimensions. We call these spanning avalanches. Since in this paper  $L_1$  and  $L_2$  are significantly smaller than  $L_3$ , it becomes quite easy for an avalanche to span the system along the thickness and width. Therefore here we take as spanning only those avalanches that span the whole system along its length.

Following Ref. [58], we fit the number  $N(R; L_1, L_2, L_3)$  of spanning avalanches per single run for the  $L_1 \times L_2 \times L_3$  systems by the model function:

$$N_{R_0, W}(R) = 0.5 \operatorname{erfc}((R - R_0)/W), \quad (2)$$

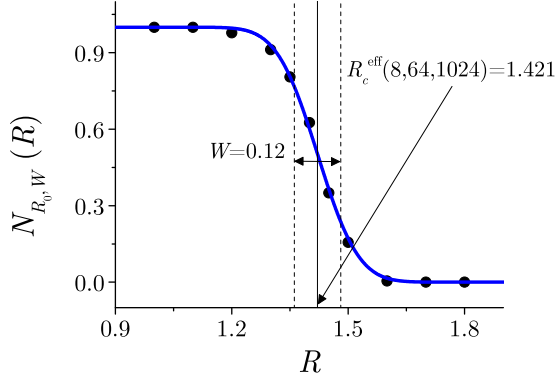


FIG. 2. Example of obtaining  $R_c^{\text{eff}}(L_1, L_2, L_3)$  in the case of lattice with  $L_1 = 8$ ,  $L_2 = 64$ , and  $L_3 = 1024$ . Black dots represent the simulation data for the number  $N(R; L_1, L_2, L_3)$  (of spanning avalanches per single run) averaged over 600 runs for each disorder, while blue line represents the fit of these data by (2).

where  $\text{erfc}(x) = (2/\sqrt{\pi}) \int_x^\infty e^{-t^2} dt$  is the complementary error function. In (2), the argument of the complementary error function is  $x = (R - R_0)/W$ , so the model function is centered at  $R = R_0$  and  $W$  is the width of its transition region (i.e., the region of disorder in which the number of spanning avalanches per single run drops from 0.75 to 0.25). Figure 2 presents how the number of spanning avalanches per single run is fitted by (2) with  $R_0 = 1.421 \pm 0.004$  and  $W = 0.12 \pm 0.01$  for the system with  $L_1 = 8$ ,  $L_2 = 64$ , and  $L_3 = 1024$ .

In general, the disorder below which the magnetization curve has jump in the thermodynamical limit for the given type of RFIM systems is called critical disorder. In finite systems the role of that disorder is played by the *effective critical disorder*  $R_c^{\text{eff}}(L_1, L_2, L_3)$  obtained as the center  $R_0 = R_c^{\text{eff}}(L_1, L_2, L_3)$  of the model function (2) that best fits the  $N(R; L_1, L_2, L_3)$  data.

Table I gives the values of effective critical disorder  $R_c^{\text{eff}}(L_1, L_2, L_3)$  for various  $L_1 \times L_2 \times L_3$  systems. It shows that the effective critical disorder for the systems of the same base  $L_1 \times L_2$  decreases with the increase of system length  $L_3$ . This is expected because it is harder for avalanches to propagate along the whole length when it becomes larger. An additional conclusion following from Table I is that  $R_c^{\text{eff}}$  increases with the increase of  $L_1 \times L_2$ . This is also expected since it is easier for an avalanche to find a way to propagate along

length if there are more “options” in the perpendicular plane. However, the question of the limit  $\lim_{L_3 \rightarrow \infty} R_c^{\text{eff}}(L_1, L_2, L_3)$  for given  $L_1$  and  $L_2$  remains, and now we will show that it is zero.

The flipping probability of a spin at disorder  $R$  and external field  $H$  is

$$p_{H,R}(S) = \int_{-(S+H)}^{\infty} \rho(h) dh = \frac{1}{2} \left[ 1 + \text{erf} \left( \frac{S+H}{R\sqrt{2}} \right) \right], \quad (3)$$

where  $\text{erf}(x) = 2/\sqrt{\pi} \int_0^x \exp(-t^2) dt$  is the standard error function, and  $S \equiv \sum_{\langle j \rangle} S_j$  is the value of the sum of the nearest-neighbor spins; in what follows we will denote this flipping probability simply by  $p(S)$ .

Let us consider the avalanche with the front (i.e., the spins flipped) at the current moment  $t_0$  composed of all  $L_1 \times L_2$  spins at the layer (i.e.,  $xy$  cross-section plane) located at  $z_0$ , and let us find the probability  $P_{L_1, L_2}$  that no spins will be flipped at the next moment  $t_0 + 1$  in the  $z_0 + 1$  cross-section plane. Using notation  $q_S = 1 - p(S)$  and taking into account that there are

- (i) 4 spins in the corners with  $S = -2$ ,
- (ii)  $2(L_1 - 2) + 2(L_2 - 2) = 2(L_1 + L_2) - 8$  spins at the edges with  $S = -3$ ,
- (iii)  $(L_1 - 2)(L_2 - 2)$  spins “in the middle” with  $S = -4$ , this probability reads

$$P_{L_1, L_2} = q_{-2}^4 q_{-3}^{2(L_1+L_2)-8} q_{-4}^{(L_1-2)(L_2-2)}. \quad (4)$$

What remained hidden in (4) is that the value of  $P_{L_1, L_2}$  also depends on  $H$  (and  $R$ ) so that it decreases when  $H$  increases. Since the spanning avalanches are almost impossible to appear at large values of  $H$ , say,  $H = 6R$ , one can conclude that the values of  $P_{L_1, L_2}$ , calculated at given  $L_1, L_2$ , and  $R$ , are bounded from below by some value  $P_{L_1, L_2}^0 > 0$ . As the probability of stopping a spanning avalanche is even greater than  $P_{L_1, L_2}$ , it follows that on average each avalanche on the strip with  $L_3 > 1/P_{L_1, L_2}^0$  will be stopped, and therefore there will be no spanning avalanches at given  $L_1, L_2$ , and  $R$ . Finally, as for the given  $L_1$  and  $L_2$ , the foregoing conclusion holds for any  $R$  it follows that  $\lim_{L_3 \rightarrow \infty} R_c^{\text{eff}}(L_1, L_2, L_3) = 0$  for that  $L_1$  and  $L_2$ .

## B. Avalanche types

Because small avalanches in  $L_1 \times L_2 \times L_3$  systems do not “see” the system’s boundaries the geometrical properties of

TABLE I. Values of effective critical disorders for various system sizes obtained as explained and shown in Fig. 2.

$L_1 \times L_2$	$R_c^{\text{eff}}(L_1, L_2, L_3)$				
	$L_3 = 256$	$L_3 = 512$	$L_3 = 1024$	$L_3 = 2048$	$L_3 = 4096$
$4 \times 16$	$0.981 \pm 0.003$	$0.821 \pm 0.003$	$0.669 \pm 0.003$	$0.554 \pm 0.003$	$0.472 \pm 0.003$
$4 \times 32$	$1.158 \pm 0.003$	$1.029 \pm 0.002$	$0.910 \pm 0.003$	$0.809 \pm 0.002$	$0.693 \pm 0.003$
$4 \times 64$	$1.266 \pm 0.003$	$1.145 \pm 0.003$	$1.049 \pm 0.003$	$0.970 \pm 0.003$	$0.926 \pm 0.004$
$8 \times 32$	$1.512 \pm 0.003$	$1.404 \pm 0.002$	$1.305 \pm 0.002$	$1.211 \pm 0.003$	$1.135 \pm 0.006$
$8 \times 64$	$1.613 \pm 0.002$	$1.505 \pm 0.002$	$1.421 \pm 0.004$	$1.350 \pm 0.002$	$1.283 \pm 0.004$
$8 \times 128$	$1.674 \pm 0.002$	$1.573 \pm 0.003$	$1.493 \pm 0.002$	$1.423 \pm 0.003$	$1.366 \pm 0.002$
$16 \times 64$	$1.843 \pm 0.002$	$1.755 \pm 0.002$	$1.677 \pm 0.002$	$1.619 \pm 0.002$	$1.562 \pm 0.002$
$16 \times 128$	$1.903 \pm 0.002$	$1.813 \pm 0.002$	$1.742 \pm 0.001$	$1.687 \pm 0.002$	$1.636 \pm 0.001$
$16 \times 256$	$1.964 \pm 0.001$	$1.847 \pm 0.001$	$1.783 \pm 0.002$	$1.729 \pm 0.001$	$1.690 \pm 0.002$

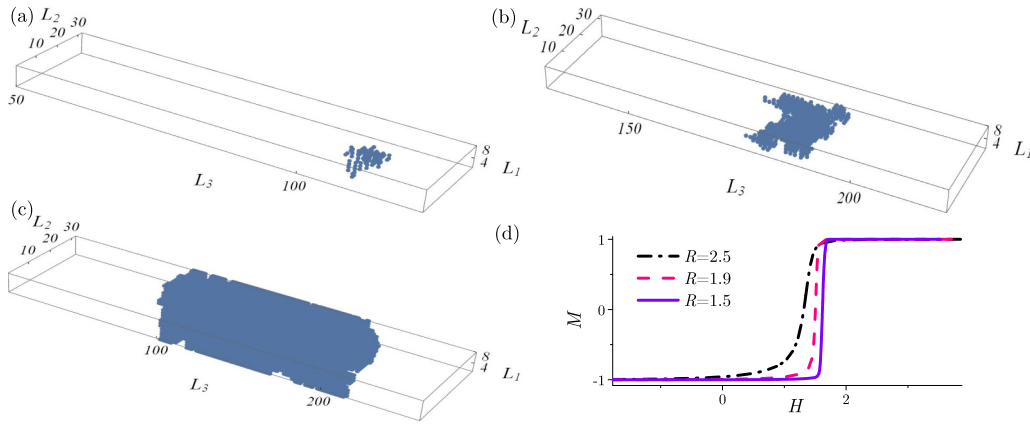


FIG. 3. Examples of different avalanche types in the  $8 \times 32 \times 256$  system. (a) A small 3-like avalanche for disorder  $R = 2.5$  at which only 3D-like avalanches appear; (b) 2D-like avalanche for  $R = 1.9$  at which only 3D-like and 2D-like avalanches appear; (c) (nonspanning) 1D-like avalanche for  $R = 1.5$  at which all types of avalanches appear; and (d) magnetization curves for three mentioned values of disorder show that a magnetization jump occurs only if 1D-like avalanches are present. Note that in (a) and (b) only part of the system is presented for better visibility.

the cluster of spins flipped in a small avalanche should be the same (in a statistical sense) as in the equilateral three-dimensional (3D) systems. The maximum size of such 3D-like avalanche is (roughly)  $L_1^{D_f}$ , where  $D_f = 1/\sigma\nu$  is the fractal dimension of nonspanning avalanches in the 3D case [49]. One 3D-like avalanche, realized at disorder  $R = 2.5$  in a  $8 \times 32 \times 256$  system, is presented in Fig. 3(a).

Avalanches larger than  $L_1^{D_f}$  typically span between the top and bottom system faces. The smaller of them propagate like 2D avalanches not touching the system's lateral sides so their size has to be less than  $L_1 L_2^2$ . One such 2D-like avalanche is presented in Fig. 3(b) for system size  $8 \times 32 \times 256$  and disorder  $R = 1.9$ .

Even larger avalanches typically span the  $L_1 \times L_2$  plane and propagate like 1D avalanches along the system's length. An example of a 1D-like avalanche is shown in Fig. 3(c) for the system size  $8 \times 32 \times 256$  and disorder  $R = 1.5$ . Note that this avalanche is nonspanning as it does not span the system along its length.

It is obvious that small 3D-like avalanches can appear in any system at any disorder. This is not the case for bigger avalanches, such as 2D-like and 1D-like, since lower values of disorder are needed for these bigger avalanches to appear.

In Fig. 4 we present how the 1D-like avalanche from Fig. 3(c) propagate along the system's length flipping practically layer by layer of spins, as argued before.

#### IV. DISTRIBUTIONS OF AVALANCHE PARAMETERS

For each avalanche one can determine its size, duration, and energy, as well as other parameters describing the avalanche. The distributions of avalanche parameters depend on the position on the hysteresis loop at which they are collected. Beside these binned-in- $H$  distributions, one is also interested in the integrated distributions pertaining to the avalanches collected along the whole hysteresis loop. All distributions in the rest of this paper are of the integrated type and the uncertainty of each distribution value is estimated by the standard error of the mean, see Ref. [59].

#### A. Distributions of avalanche size

Let us first describe the avalanche distributions for the RFIM system of a given size  $L_1 \times L_2 \times L_3$ .

At disorders  $R$  much larger than  $R_c^{\text{eff}}(L_1, L_2, L_3)$  only 3D-like avalanches appear and the shapes of distributions are like in equilateral 3D model. In the case of size distribution, this is illustrated in the main part of Fig. 5(a) for the system of size  $8 \times 64 \times 4096$ . Here the value of size exponent for various disorders is the same within the error bars  $\tau_{3D} = 1.70 \pm 0.01$ .

Next, as  $R$  decreases from large values toward  $R_c^{\text{eff}}(L_1, L_2, L_3)$ , the 2D-like avalanches also appear. Therefore, as in the case illustrated in Fig. 5(b), the shape of distributions is transformed from a power law into a double power law [16] both ending with cutoff. The initial part of this double power law comes from 3D-like avalanches and bends at  $S \approx 300 \approx L_1^{D_f} = S_{\text{max}}^{3D}$  into the second power law that (almost entirely) comes from 2D-like avalanches. The second part is described by the second effective exponent, here  $\tau_{2D} = 1.32 \pm 0.01$ , which turns out to be the same for all disorders in questions, see Fig. 5(b). However, although one could expect that the slopes in the  $S < S_{\text{max}}^{3D}$  region should be also the same and equal to  $\tau_{3D}$  for all distributions, this is not the case because the lower the disorder, the easier it is for an avalanche that is expected to be 3D-like to become 2D-like.

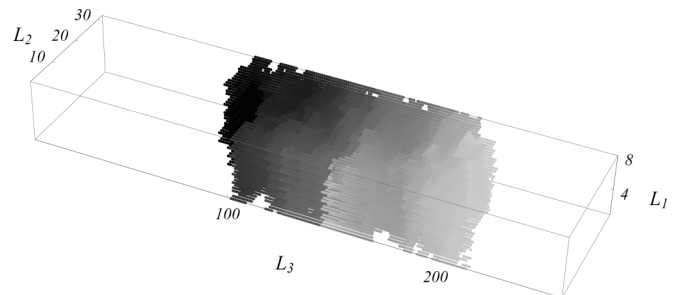


FIG. 4. One-dimension-like avalanche evolution in system of size  $8 \times 32 \times 256$  and disorder  $R = 1.5$ . Darker sites represent spins that flipped earlier.

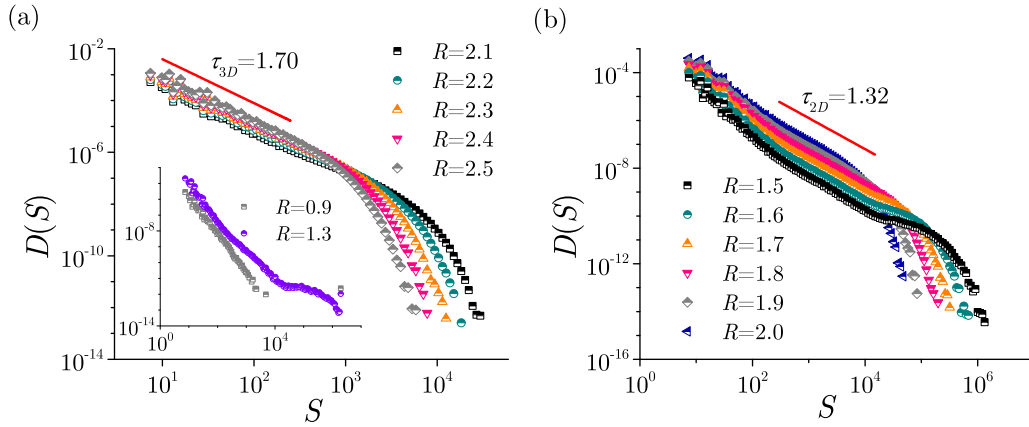


FIG. 5. Log-log plot of distributions  $D(S)$  of avalanche size  $S$  for the  $8 \times 64 \times 4096$  system; the number of different random-field configurations used in averaging ranged from 400 for largest up to 4000 for lowest disorders. (a) In disorder range from  $R = 2.1$  to  $R = 2.5$  only 3D avalanches appear (slope of the linear part of curves is  $-1.7$ ); spanning avalanches appear for  $R = 0.9$  and  $R = 1.3$  as shown in inset. (b) For disorders from  $R = 1.5$  to  $R = 2.0$ , both 2D-like and 3D-like avalanches appear, while 1D-like avalanches are absent; the slope of the linear middle part of curves is  $-1.32$ .

That happens due to finite values of  $L_1$  and  $L_2$ , so when an avalanche reaches borders along these directions it comes in contact with spins that have fewer nearest neighbors, which, in combination with a small disorder, make those spins easier to become unstable and flip. This is why there are fewer larger 3D avalanches as the disorder lowers, which consequently makes the slope steeper in the  $S < S_{\max}^{3D}$  range.

Finally, the avalanches of size greater than the maximum size  $S_{\max}^{2D} \propto L_1 L_2^2$  for 2D-like avalanches, here  $S_{\max}^{2D} \approx 32\,000$ , propagate as 1D-like avalanches which contribute to the tails of distributions presented in Fig. 5(b). Distributions collected at disorders  $R < R_c^{\text{eff}}(L_1, L_2, L_3)$ , see the inset in Fig. 5(a), have a jump at the very end caused by the spanning avalanche that appears in almost each run, whose size is only slightly smaller than the total number of spins in the system, here  $\approx 2 \times 10^6$ .

Having demonstrated how the value of disorder influences the shape of avalanche size distributions for the systems of the same size, let us now show how the system size affects this shape at the same disorders. In Fig. 6 are presented the avalanche size distributions for two systems of size  $8 \times 32 \times 256$  and  $4 \times 64 \times 1024$  at the same disorder  $R = 2.0$ . The slopes of both solid and both dashed lines have the same values,  $-1.7$  and  $-1.32$ , corresponding to the distribution parts dominated by the 3D-like and 2D-like avalanches, respectively. Still, the distributions are significantly different particularly because of different extent of 3D and 2D parts.

### B. Distributions of avalanche duration

The shapes of avalanche duration distributions follow the same trend as the avalanche size distributions. Their initial parts are dominated by the 3D-like, middle parts by the 2D-like, and ends by the 1D-like avalanches. The extent of these parts vary with disorder so that for disorders far above the effective critical disorder  $R_c^{\text{eff}}(L_1, L_2, L_3)$  only the 3D part is visible, for lower disorders that are still above  $R_c^{\text{eff}}(L_1, L_2, L_3)$  the 2D part and nonspanning 1D part appear, and, finally, the spanning 1D part appears below  $R_c^{\text{eff}}(L_1, L_2, L_3)$ .

Figure 7(a) shows five duration distributions for the system of size  $8 \times 64 \times 4096$  and disorders  $R = 1.2, 1.6, 1.8, 2.2, 2.4$ , respectively. One can notice here that for the two biggest disorders when only 3D-like avalanches appear the distributions follow a power law specified by the exponent  $\alpha_{3D} = 2.20 \pm 0.01$ . This shape persists as long as duration of all triggered avalanches is less than  $T_{\max}^{3D} \propto L_1^z$ , where  $z$  is the dynamical critical exponent in the three-dimensional model [15]. If this is not the case, then the 2D-like, together with 3D-like, avalanches are triggered, and the shape of distributions gradually transforms into double power law. The second power law that corresponds to the 2D-like avalanches is characterized by the exponent  $\alpha_{2D} = 1.63 \pm 0.01$ . Last, at disorders below the effective

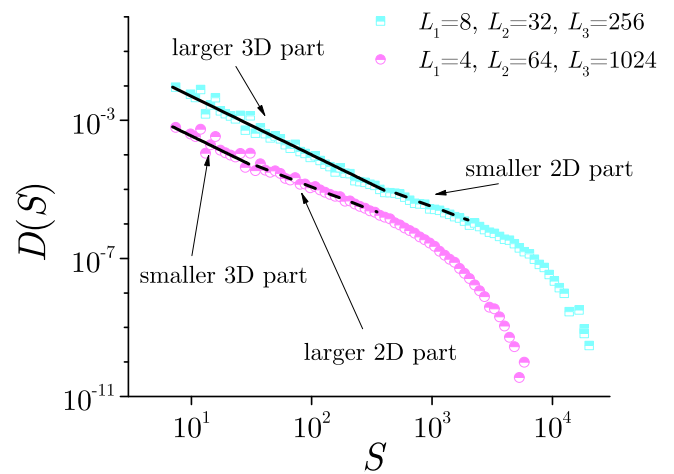


FIG. 6. Avalanche size distributions for the systems of size  $8 \times 32 \times 256$  (squares) and  $4 \times 64 \times 1024$  (circles). Disorder for both systems is  $R = 2.0$ . Solid lines, whose slopes are  $-1.7$  represent the parts with 3D avalanches, while dashed lines, whose slopes are  $-1.32$ , represent the parts with 2D-like avalanches. Values of the  $8 \times 32 \times 256$  curve have been shifted upward (multiplied by 20) to make the image clearer.

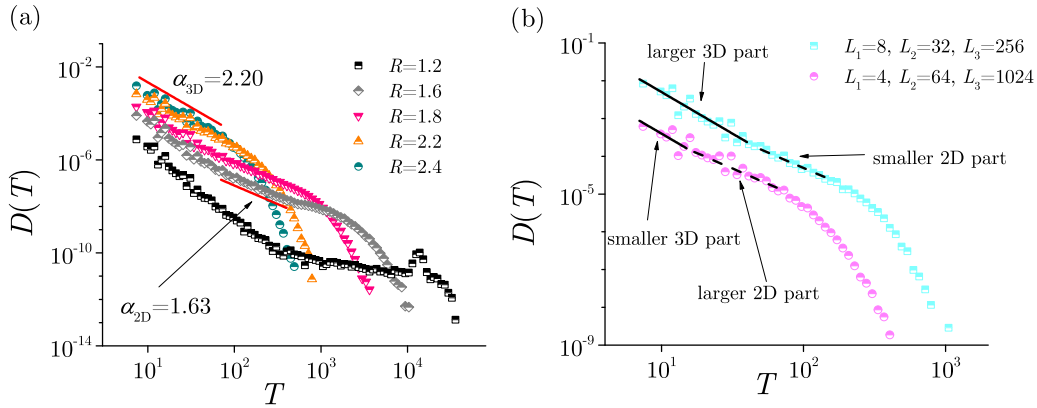


FIG. 7. (a) Avalanche duration distributions for the system of size  $8 \times 64 \times 4096$  and five different disorders  $R = 1.2$ ,  $R = 1.6$ ,  $R = 1.8$ ,  $R = 2.2$ , and  $R = 2.4$ . Solid lines represent slopes of 3D and 2D-like avalanches, whose values are  $-2.2$  and  $-1.63$  respectively. (b) Avalanche duration distributions for the systems of size  $8 \times 32 \times 256$  (squares) and  $4 \times 64 \times 1024$  (circles), with same disorders,  $R = 2.0$ . Solid lines, whose slopes are  $-2.2$ , represent the parts with 3D avalanches, while dashed lines, whose slopes are  $-1.63$ , represent the parts with 2D-like avalanches. Values of the  $8 \times 32 \times 256$  curve have been shifted upward (multiplied by 20) to make the image clearer.

critical disorder spanning 1D-like avalanches are triggered as well, and a peak arises at the far end of the curve.

Figure 7(b) presents two duration distributions for the  $8 \times 32 \times 256$  and  $4 \times 64 \times 1024$  systems, and the same disorder  $R = 2.0$ , that behave like the size distributions shown in Fig. 6.

### C. Distributions of avalanche energy

In Fig. 8 we present the avalanche energy distributions. These distributions behave like the size and duration distributions from two previous subsections. Thus, the distributions shown in Fig. 8(a) are obtained for the  $8 \times 64 \times 4096$  system at five different disorders. The distributions for the two largest disorders are of a power-law type specified by the exponent  $\epsilon_{3D} = 1.53 \pm 0.01$  and are due to 3D-like avalanches only. At lower disorders 2D-like avalanches appear, giving a dominant contribution in the middle part of distributions starting at energy that is greater than  $E_{\max}^{3D}$ , where  $E_{\max}^{3D} \propto L_1^{\gamma_{E/S} D_f}$  and  $\gamma_{E/S}$  is the exponent that describes how avalanche energy de-

pends on avalanche size ( $E$ )  $\sim S^{\gamma_{E/S}}$  [15]. The power-law part that corresponds to two 2D-like avalanches is characterized by the exponent  $\epsilon_{2D} = 1.21 \pm 0.01$ . For disorders below the effective critical disorder a peak arises at the far end of the distribution curve caused by the spanning avalanche.

Figure 8(b) shows energy distributions for systems with different sizes,  $8 \times 32 \times 256$  (squares) and  $4 \times 64 \times 1024$  (circles), and the same disorder  $R = 2.0$ . These curves show that not only disorder but also the system size affects the distribution shape, since the extent of 3D-like and 2D-like parts varies greatly.

### V. SCALING OF AVALANCHE DISTRIBUTIONS

To achieve proper scaling of distributions of avalanche parameters for  $L_1 \times L_2 \times L_3$  striplike systems it is convenient to start from the general scaling relation (5) for the joint distribution  $D(S, T, E; h', r, 1/L_1, 1/L_2, 1/L_3)$  of size  $S$ , duration  $T$ , and energy  $E$  of avalanches collected at reduced magnetic field  $h'$  and reduced disorder  $r$ , which integrated

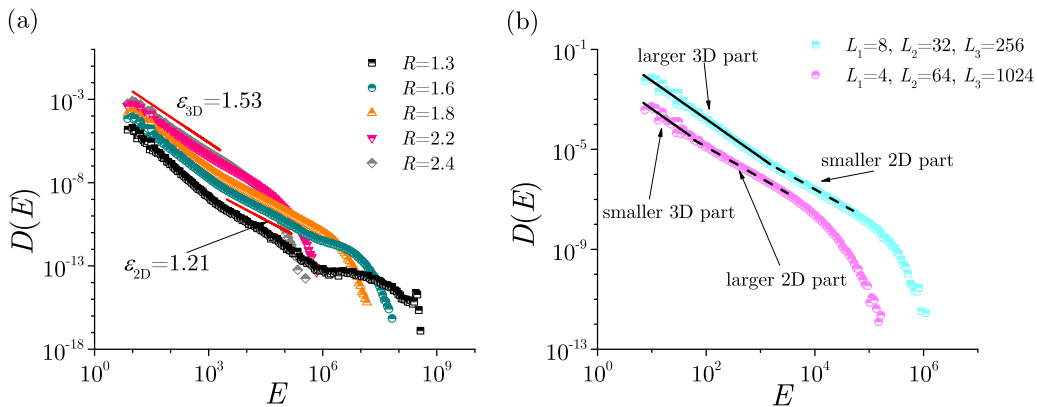


FIG. 8. (a) Avalanche energy distributions for the system of size  $8 \times 64 \times 4096$  and five different disorders  $R = 1.3$ ,  $R = 1.6$ ,  $R = 1.8$ ,  $R = 2.2$ , and  $R = 2.4$ . Solid lines mark the 3D-like and 2D-like parts having slopes  $-1.53$  and  $-1.21$ , respectively. (b) Avalanche energy distributions for the systems of size  $8 \times 32 \times 256$  (squares) and  $4 \times 64 \times 1024$  (circles), with the same disorders,  $R = 2.0$ . Solid lines, whose slopes are  $-1.53$ , represent the parts with 3D avalanches, while dashed lines, whose slopes are  $-1.21$ , represent the parts with 2D-like avalanches. Values of the  $8 \times 32 \times 256$  curve have been shifted upward (multiplied by 20) for better visibility.

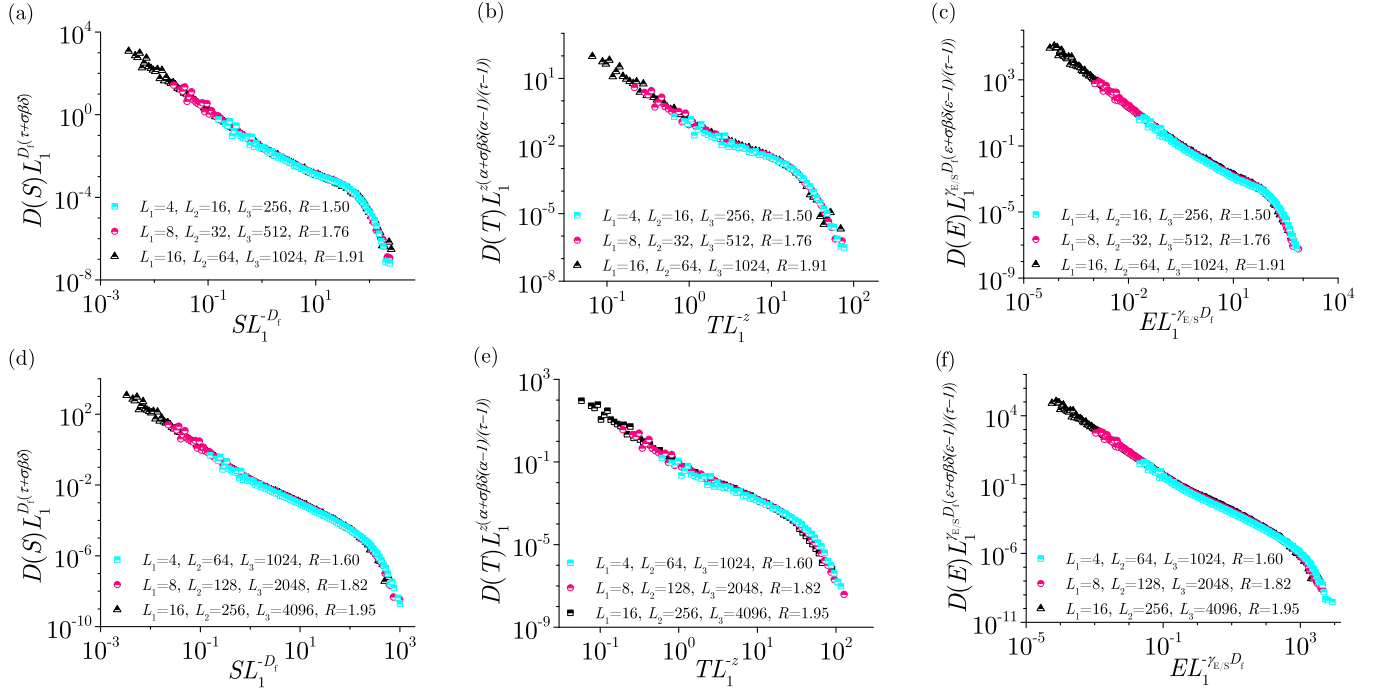


FIG. 9. Collapsing of avalanche size distributions using (11) in (a) and (d), duration distributions using (13) in (b) and (e), and energy distributions in (c) and (f) using (14). The employed values for  $L_1:L_2:L_3$  are as follows: 1:4:64 in (a) and 1:16:256 in (d), 1:4:64 in (b) and 1:16:256 in (e), and 1:4:64 in (c) and 1:16:256 in (f). The values of disorder  $R$  are adjusted to achieve the constant value of  $L^{1/\nu}r$  for all distributions from the same panel.

over the entire hysteresis loop gives (6). Here  $r = R/R_c^{3D} - 1$ , and  $h' = H - H_c + Br$ , where  $R_c^{3D} = 2.16$  and  $H_c = 1.435$  are the critical disorder and critical field of 3D model on equilateral lattices, while  $B = 0.39$  is the “rotation” parameter keeping track of the shifting of the susceptibility curves maxima. Additionally, in the present section, the standard RFIM exponents, expressed in (7)–(9) in terms of nonstandard exponents from (5) and (6), are given the values from the 3D model [35,46–48,60],

$$D(\lambda^{a_S} S, \lambda^{a_T} T, \lambda^{a_E} E; \lambda^{b_h} h', \lambda^{b_r} r, \lambda^{b_{L_1}}/L_1, \lambda^{b_{L_2}}/L_2, \lambda^{b_{L_3}}/L_3) = \lambda D(S, T, E; h', r, 1/L_1, 1/L_2, 1/L_3); \quad (5)$$

$$D(\lambda^{a_S} S, \lambda^{a_T} T, \lambda^{a_E} E; \lambda^{b_r} r, \lambda^{b_{L_1}}/L_1, \lambda^{b_{L_2}}/L_2, \lambda^{b_{L_3}}/L_3) = \lambda^{1+b_h} D(S, T, E; r, 1/L_1, 1/L_2, 1/L_3); \quad (6)$$

$$\tau = 1 - \frac{1+a}{a_S}, \quad \alpha = 1 - \frac{1+a}{a_T}, \quad \epsilon = 1 - \frac{1+a}{a_E}; \quad (7)$$

$$a = a_S + a_T + a_E, \quad \frac{a}{1+a} = \frac{1}{1-\tau} + \frac{1}{1-\alpha} + \frac{1}{1-\epsilon}; \quad (8)$$

$$b_r = -a_S\sigma, \quad b_h = -a_S\sigma\beta\delta, \quad b_L = -a_S\sigma\nu. \quad (9)$$

By integrating (6) over  $T$  and  $E$  we get the scaling prediction

$$D(\lambda^{a_S} S; \lambda^{b_r} r, \lambda^{b_{L_1}}/L_1, \lambda^{b_{L_2}}/L_2, \lambda^{b_{L_3}}/L_3) = \lambda^{1+a-a_S+b_h} D(S; r, 1/L_1, 1/L_2, 1/L_3), \quad (10)$$

for the avalanche size distribution and subsequently

$$D\left(\frac{S}{L_1^{D_f}}; L_1^{1/\nu} r, 1, \frac{L_1}{L_2}, \frac{L_1}{L_3}\right) = L_1^{\tau D_f} D\left(S; r, \frac{1}{L_1}, \frac{1}{L_2}, \frac{1}{L_3}\right), \quad (11)$$

by using (7), (8), (9), (10), and  $\tau' = \tau + \sigma\beta\delta (= 2.03)$ , taking that

$$\lambda = L_1^{-D_f/a_S}, \quad (12)$$

so that the avalanche size  $S$  rescales its biggest value  $S_{\max}^{3D} \propto L_1^{D_f}$  for the 3D-like avalanches. For the systems with the same aspect ratios  $L_1/L_2$  and  $L_1/L_3$  at disorders providing the same value of  $rL_1^{1/\nu}$ , (11) implies that the size distribution curves multiplied by  $L_1^{\tau D_f}$  should collapse onto one curve when presented against  $S/L_1^{D_f}$ . This is shown in Figs. 9(a) and 9(b), where  $L_1/L_2 = 1/4$ ,  $L_1/L_3 = 1/64$ ,  $rL_1^{1/\nu} = -0.82$  and  $L_1/L_2 = 1/16$ ,  $L_1/L_3 = 1/256$ ,  $rL_1^{1/\nu} = -0.7$ , both for  $1/\nu = 0.71$ .

In an analogous way, one can derive the scaling predictions for the avalanche duration and avalanche energy distributions by choosing  $\lambda = L_1^{-z/a_T}$  for duration and  $\lambda = L_1^{-\gamma_{E,S}D_f/a_E}$  for avalanche energy. Thus, the scaling prediction for avalanche duration distribution reads

$$D(T/L_1^z; L_1^{1/\nu} r, 1, L_1/L_2, L_1/L_3) = L_1^{z(\alpha+\sigma\beta\delta(\alpha-1)/(\tau-1))} D(T; r, 1/L_1, 1/L_2, 1/L_3), \quad (13)$$

while for avalanche energy distribution is

$$\begin{aligned} D(E/L_1^{\gamma_E/\delta D_f}; L_1^{1/\nu} r, 1, L_1/L_2, L_1/L_3) \\ = L_1^{\gamma_E/\delta D_f(\epsilon+\sigma\beta\delta(\epsilon-1)/(\tau-1))} D(T; r, 1/L_1, 1/L_2, 1/L_3). \end{aligned} \quad (14)$$

Figures 9(b) and 9(e) present the collapses of duration distributions, and Figs. 9(c) and 9(f) present energy distributions obtained for the same system parameters as for the size distributions.

## VI. EFFECTIVE CRITICAL FIELD

In response to variation of the external magnetic field  $H$ , the magnetization  $M$  of the RFIM spin system changes at the rate  $\chi = dM/dH$ , called susceptibility; for another definition of susceptibility in RFIM, see Refs. [61,62]. The value of  $H$  at which the system susceptibility curve, taken at the current disorder  $R$ , attains its maximum, which we take as the effective critical field  $H_c^{\text{eff}}(R)$  of the system at disorder  $R$ . Besides  $R$ , the effective critical field depends on the system size, but this is omitted in its notation for the sake of simplicity.

Two examples of the susceptibility curves  $\chi = \chi(H)$ , obtained by averaging 10 000 different random-field configurations, are given in Fig. 10. The curves correspond to the  $4 \times 16 \times 4096$  system at disorders  $R = 0.6$  in Fig. 10(a) and  $R = 1.1$  in Fig. 10(b). In Fig. 10(a)  $H_c^{\text{eff}} = 2.18 \pm 0.05$ , and  $H_c^{\text{eff}} = 1.80 \pm 0.04$  in Fig. 10(b), with the error bars calculated as half of the maximum absolute deviation of  $H_c^{\text{eff}}(R)$  from the ordinates of maxima of the single run susceptibilities. The insets in Fig. 10 present the sample-to-sample variations of the susceptibility curves which are smaller for larger disorder, leading to a smoother curve. The values of  $H_c^{\text{eff}}(R)$ , obtained in this way, are presented in Figs. 11(a), 11(b) and 11(c) for the systems with the same  $L_1$  and  $L_2$  but different  $L_3$ , while in Figs. 11(d), 11(e) and 11(f) show the data for the systems with the same  $L_3$  but different  $L_1$  and  $L_2$ .

Let us first point out that for small  $R$ , the effective critical disorder depends linearly on  $R$  for all *finite* striplike systems studied in this paper. Indeed, all spins in such systems are initially set to  $S_i = -1$  and remain stable at  $R = 0$  until the external magnetic field grows from  $H = -\infty$  to  $H = +4$ . At this value of  $H$  all spins at the system edges flip because they have only four nearest neighbors. Their flipping destabilizes all of their nearest neighbors which will flip in the next moment of time destabilizing all of their nearest neighbors, and so on, creating thus a *single* avalanche that flips *all* spins in the system.

Having the smallest number of nearest neighbors (=4), the spins at system edges are the first candidates for flipping at any  $R$  because of the greatest flipping probability  $p(-4)$ , see (3). For

$$H \geq 4 - R\sqrt{2}\text{erf}^{-1}\left(1 - \frac{2}{4L_3}\right), \quad (15)$$

where  $\text{erf}^{-1}(x)$  is the inverse error function, it follows that

$$p(-4) \geq \frac{1}{4L_3}, \quad (16)$$

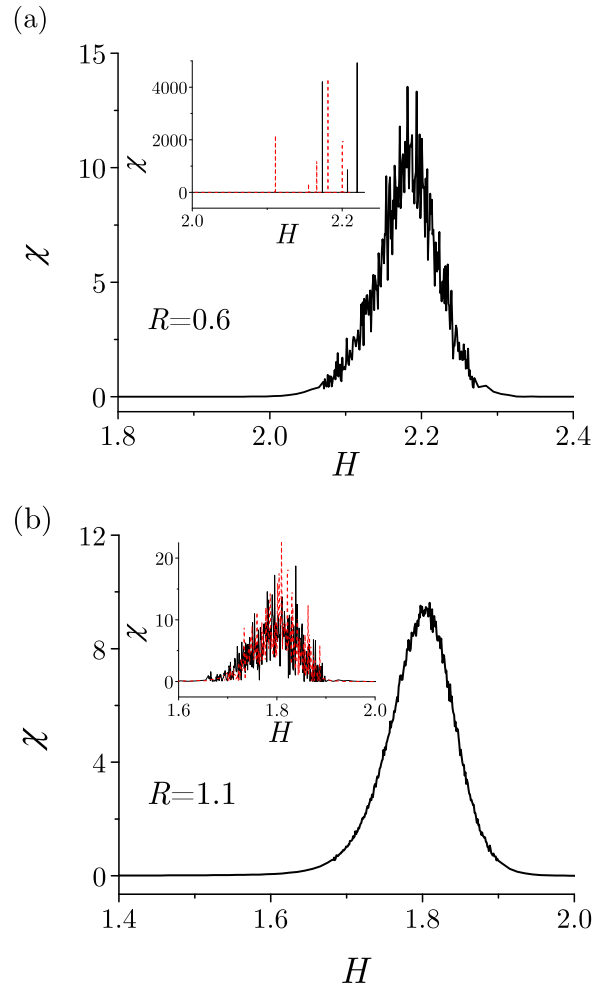


FIG. 10. Susceptibility curves for the  $4 \times 16 \times 4096$  system averaged over 10 000 different random-field configurations (main panels) and for two single runs, presented in solid black line and dashed red line in insets. The curves in (a) are obtained at disorder  $R = 0.6$  and at  $R = 1.1$  in (b).

so at least one of the edge spins will flip on average. The flipping of an edge spin  $S_i$  causes the sum of nearest-neighbor spins  $\sum_{(i,j)} S_j$  for each of its edge nearest neighbors  $S_j$  to be  $-2$  at least. So if not already flipped, then  $S_i$  will flip because its flipping probability  $p(-2)$  at  $H \approx 4$  is almost 1 if disorder  $R$  is sufficiently small. In this way the flipping of single edge spin results at sufficiently small disorder in flipping of all spins located at the same edge. This holds for all four system edges and, in a further consequence, leads to emergence of a spanning avalanche. For all of the foregoing reasons, at sufficiently small disorder  $R$ , the effective critical field is a linear function

$$H_c^{\text{eff}}(R) = 4 - R\sqrt{2}\text{erf}^{-1}\left(1 - \frac{2}{4L_3}\right), \quad (17)$$

of  $R$  with the y intercept equal to 4 and gradient  $-\sqrt{2}\text{erf}^{-1}(1 - 2/4L_3)$ , as is confirmed by Fig. 11.

Besides  $H_c^{\text{eff}}(R)$ , one can calculate the value  $H(R, L_3)$  of the external field at which it is *likely* that all spins at an edge will be flipped if a *single* spin is already flipped at that



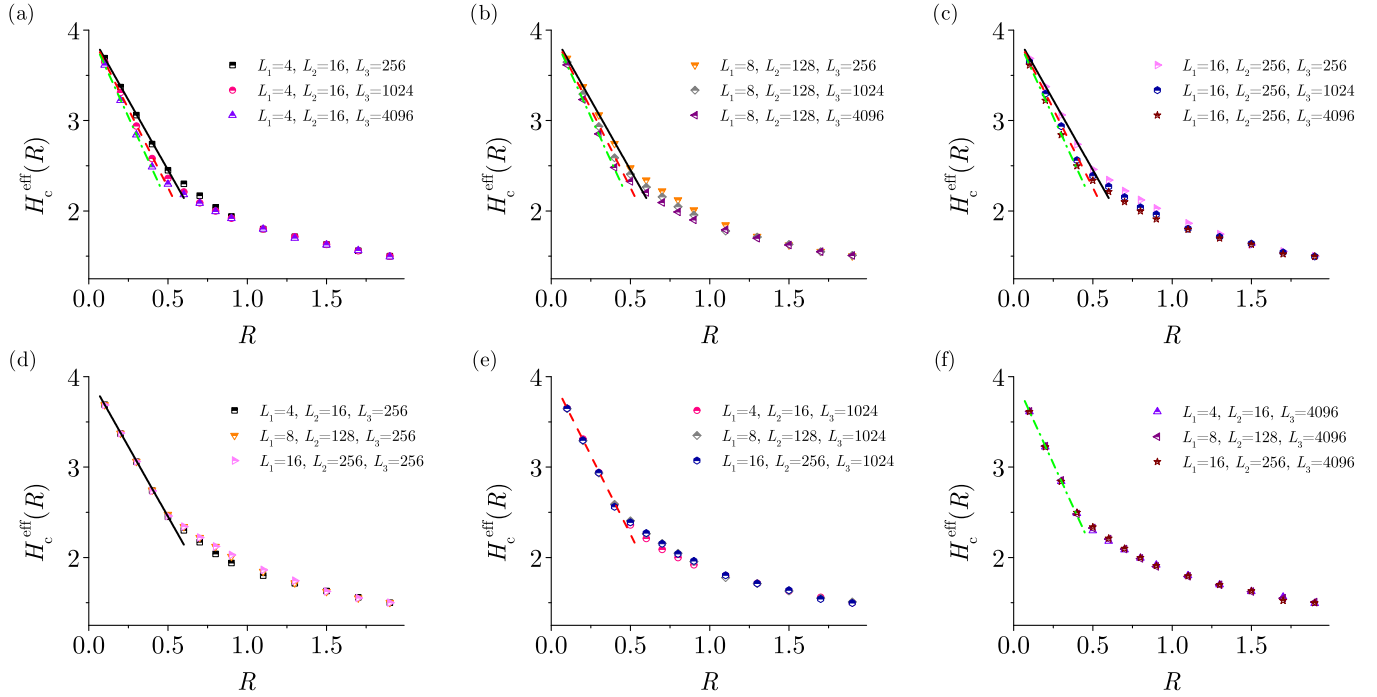


FIG. 11. Critical external fields for disorders in range from  $R = 0.1$  to  $R = 1.9$ . In upper panels  $L_1$  and  $L_2$  are the same, while  $L_3$  ranges from 256 to 4096; (a)  $L_1 = 4, L_2 = 16$ ; (b)  $L_1 = 8, L_2 = 128$ ; and (c)  $L_1 = 16, L_2 = 256$ . In lower panels  $L_3$  is the same while  $L_1 \times L_2$  take values  $4 \times 16$ ,  $8 \times 128$ , and  $16 \times 256$ ; (d)  $L_3 = 256$ ; (e)  $L_3 = 1024$ ; (f)  $L_3 = 4096$ . Straight lines represent linear dependence  $H_c(R)$  given by (17) for  $L_3 = 256$  (solid line),  $L_3 = 1024$  (dashed line), and  $L_3 = 4096$  (dash-dotted line).

edge. To this end, let us consider the avalanches triggered by flipping by the external field  $H$  one of the two nearest neighbors of the flipped spin that are located at the edge. The number  $L$  of spins comprising such avalanche can take the value from  $L = 1$  (when none of the two neighbors is flipped by  $H$ ) to  $L = L_3$  (when all spins at the edge are flipped by  $H$ ). Now let the index  $l$  counts the spins at the edge starting from  $l = 0$  at the flipped spin so  $l = 1$  and  $l = L_3 - 1$  are its two nearest edge neighbors. The probability  $p_1$  that  $H$  will not flip any edge spin (of having only *one* flipped spin at the edge) is  $p_1 = q^2$ ; here  $q = 1 - p$  and  $p$  is the flipping probability by  $H$  of an edge spin having one flipped neighbor. Likewise, the probability of having  $L$  flipped spins at the edge is  $p_L = Lp^{L-1}q^2$  for  $1 \leq L \leq L_3 - 2$ . On the other hand, if  $L_3 - 1$  edge spins are already flipped by  $H$ , then the remaining spin having two flipped edge neighbors will almost surely flip as well, giving  $p_{L_3} = (L_3 - 1)p^{L_3-2}$ . Thus, when  $p_{L_3} > \sum_{l=1}^{L_3-2} p_l$ , one may say that it is likely that all edge spins are flipped by  $H$ , which gives that

$$(L_3 - 1)p^{L_3-2} = q^2 \sum_{l=1}^{L_3-2} lp^{l-1}, \quad (18)$$

is satisfied at  $H = H(R, L_3)$ . The field  $H(R, L_3)$ , numerically determined from (18) for  $L_3 = 1024$  and  $p = p_{H(R, L_3), R}(-2)$  given by (3), is shown versus disorder  $R$  in Fig. 12 together with  $H_c^{\text{eff}}(R)$ , see (17). For  $R \lesssim 0.37$ ,  $H_c^{\text{eff}}(R) \geq H(R, L_3 = 1024)$ , showing that the first flipping of edge spin occurring at  $H = H_c^{\text{eff}}(R)$  continues into a spanning avalanche and, therefore, such disorders can be taken as *small*. For higher disorders, more than one edge spin has to be flipped,

meaning that  $H_c^{\text{eff}}(R) > 4 - R\sqrt{2}\text{erf}^{-1}(1 - \frac{2}{4L_3})$  but less than  $H(R, L_3)$ , giving an upper bound for creation of spanning avalanche by flipping of an additional edge spin.

At the opposite end, more precisely for  $R \gtrsim 1.5$ , the curves shown in Fig. 11 merge, meaning that the susceptibility curves at each such value of disorder attain their maximum at the same value of  $H$  irrespectively of the system size which happens because then the entire system response becomes independent on the system size.

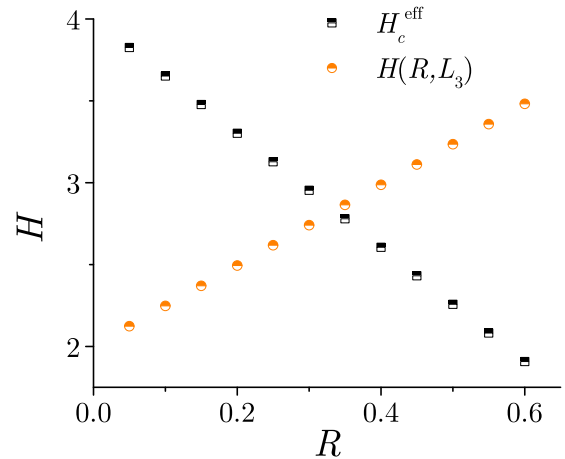


FIG. 12. System length is  $L_3 = 1024$ . Squares represent external field needed for the first spin to flip, obtained from (17). Circles show the values of external field needed for the biggest avalanche to appear, obtained from (18).

In the intermediate range of disorder the curves for different system sizes diverge so that (1) for the curves corresponding to the same values of  $L_1$  and  $L_2$ , the greater the  $L_3$ , the lower the  $H_c^{\text{eff}}(R)$  (because it is easier to trigger the largest avalanche at longer edge), and (2) conversely, for larger  $L_1$  and  $L_2$  but same  $L_3$ , because then it is easier to trigger all spins from the  $L_1 \times L_2$  planes.

## VII. DISCUSSION

Our findings from previous sections may have significant implications for data analysis of Barkhausen noise experiments performed on striplike samples. Reported values of the critical exponents, estimated from experimental avalanche distributions, are (1) roughly equal to the (absolute value of) slope of the scaling region of the distribution's log-log plot and (2) vary from experiment to experiment. Although differences in these values may originate in a vast variety of reasons, here we argue that they may be to some extent also attributed to the different geometrical aspects of the employed samples.

Also, we believe that our findings might give a clue as to what the relative values of disorder in real systems are, i.e., to tell which of two systems has a greater disorder.

Thus, the experimental values of avalanche size exponent and avalanche duration exponent,  $\tau_{\text{exp}} = 1.73$  and  $\alpha_{\text{exp}} = 2.28$ , are reported in Ref. [1],  $\tau_{\text{exp}} = 1.77$  and  $\alpha_{\text{exp}} = 2.22$  in Ref. [2], and  $\tau_{\text{exp}} \approx 1.3$  and  $\alpha_{\text{exp}} = 1.5$  in Refs. [3–5,9]. We report approximately the same values for the pair  $\tau_{3\text{D}}$ ,  $\alpha_{3\text{D}}$  describing the 3D-like avalanches, see Fig. 5(a) and Fig. 7(a), and for the pair  $\tau_{2\text{D}}$ ,  $\alpha_{2\text{D}}$  describing the 2D-like avalanches, see Fig. 5(b) and Fig. 7(a), which opens the door for speculating that this could be due to an interplay between geometrical aspects and disorder. So for the samples that are either thick enough and/or with large disorder, the 3D-like avalanches are dominantly present, causing the advent of  $\tau_{3\text{D}}$ -like and  $\alpha_{3\text{D}}$ -like values of exponents, whereas 2D-like avalanches, and therefore  $\tau_{2\text{D}}$ -like and  $\alpha_{2\text{D}}$ -like values of exponents, appear in the opposite case.

The foregoing similarities are followed, however, by important differences possibly coming from rather smaller experimental aspect ratios  $L_1/L_2$  and  $L_1/L_3$  which might result

in a shorter 3D part. In addition, the small avalanches from the 3D part are, much more than larger avalanches, affected (or even hidden) by the concomitant noise, overall resolution, and choice of threshold level in experiments. Together with smaller experimental aspect ratios, this may cause the absence of bending between the 3D-like and 2D-like behaviors in experimental distributions.

## VIII. CONCLUSION

In conclusion, we presented a study of behavior of the athermal nonequilibrium random-field Ising model in adiabatic regime of spins located at the striplike  $L_1 \times L_2 \times L_3$  cubic lattices with  $L_1 < L_2 < L_3$ , using closed boundary conditions along their length  $L_3$  and open along thickness  $L_1$  and width  $L_2$ . The smallest avalanches in such systems are unaffected by the boundaries and are, therefore, classified as 3D like. Larger avalanches spread between the bottom and top faces of the system and propagate as in 2D systems, whereas the largest avalanches are classified as 1D like because they advance along the system length by flipping almost all spins from the cross section at the avalanche front. The presence of these avalanche types is manifested in the shape of distributions of avalanche size, duration, and energy as 3D-like, 2D-like, and 1D-like parts having different slopes (i.e., effective exponents) and extent controlled by disorder  $R$ . The distributions are collapsible following the derived finite-size scaling laws which employ aspect ratios  $L_1/L_2$ ,  $L_1/L_3$ , and the (standard choice for) reduced disorder  $r = R/R_c - 1$ . Here  $R_c$  is the critical disorder not for this model (which is zero according to the provided evidences) but for the 3D model on the equilateral lattices. Besides the effective critical disorder, we have also determined the behavior of the effective critical field (i.e., the field triggering the biggest avalanche) for the finite striplike systems and provided its analytic expression in the range of small disorders. Finally, we discussed the relevance that our findings might have for the interpretation of the Barkhausen noise experimental data.

## ACKNOWLEDGMENT

This work was supported by the Serbian Ministry of Education, Science and Technological Development.

- 
- [1] U. Lieneweg and W. Grosse-Nobis, *Int. J. Magn.* **3**, 11 (1972).
  - [2] Dj. Spasojević, S. Bukvić, S. Milošević, and H. E. Stanley, *Phys. Rev. E* **54**, 2531 (1996).
  - [3] G. Durin and S. Zapperi, *Phys. Rev. Lett.* **84**, 4705 (2000).
  - [4] D. H. Kim, S. B. Choe, and S. C. Shin, *Phys. Rev. Lett.* **90**, 087203 (2003).
  - [5] S. C. Shin, K. S. Ryu, D. H. Kim, S. B. Choe, and H. Akinaga, *J. Magn. Magn. Mater.* **310**, 2599 (2007).
  - [6] K. S. Ryu, H. Akinaga, and S-Ch. Shin, *Nat. Phys.* **3**, 547 (2007).
  - [7] A. Benassi and S. Zapperi, *Phys. Rev. B* **84**, 214441 (2011).
  - [8] G. Z. dos Santos Lima, G. Corso, M. A. Correa, R. L. Sommer, P. Ch. Ivanov, and F. Bohn, *Phys. Rev. E* **96**, 022159 (2017).
  - [9] F. Bohn, G. Durin, M. A. Correa, N. Ribeiro Machado, R. DominguesDella Pace, C. Chesman, and R. L. Sommer, *Sci. Rep.* **8**, 11294 (2018).
  - [10] P. Cizeau, S. Zapperi, G. Durin, and H. E. Stanley, *Phys. Rev. Lett.* **79**, 4669 (1997).
  - [11] S. Zapperi, P. Cizeau, G. Durin, and H. E. Stanley, *Phys. Rev. B* **58**, 6353 (1998).
  - [12] L. Laurson, G. Durin, and S. Zapperi, *Phys. Rev. B* **89**, 104402 (2014).
  - [13] V. Estevez and L. Laurson, *Phys. Rev. B* **91**, 054407 (2015).
  - [14] V. Estevez and L. Laurson, *Phys. Rev. B* **93**, 064403 (2016).

- [15] Dj. Spasojević, S. Mijatović, V. Navas-Portella, and E. Vives, *Phys. Rev. E* **97**, 012109 (2018).
- [16] B. Tadić, S. Mijatović, S. Janičević, Dj. Spasojević, and G. J. Rodgers, *Sci. Rep.* **9**, 6340 (2019).
- [17] A. Skaugen, P. Murray, and L. Laurson, *Phys. Rev. B* **100**, 094440 (2019).
- [18] S. Mijatović, D. Jovković, S. Janičević, and Dj. Spasojević, *Phys. Rev. E* **100**, 032113 (2019).
- [19] N. Friedman, S. Ito, B. A. W. Brinkman, M. Shimono, R. E. L. DeVille, K. A. Dahmen, J. M. Beggs, and T. C. Butler, *Phys. Rev. Lett.* **108**, 208102 (2012).
- [20] C. Bedard, H. Kroger, and A. Destexhe, *Phys. Rev. Lett.* **97**, 118102 (2006).
- [21] J. Davidsen and M. Baiesi, *Phys. Rev. E* **94**, 022314 (2016).
- [22] T. Makinen, A. Miksic, M. Ovaska, and M. J. Alava, *Phys. Rev. Lett.* **115**, 055501 (2015).
- [23] J. P. Bouchaud, *J. Stat. Phys.* **151** 567 (2013).
- [24] D. P. Belanger, in *Spin Glasses and Random Fields*, edited by A. P. Young (World Scientific, Singapore, 1998).
- [25] J. P. Sethna, K. A. Dahmen, O. Perković, in *The Science of Hysteresis*, edited by G. Bertotti and I. Mayergoyz (Academic Press, Amsterdam, 2006).
- [26] K. A. Dahmen, J. P. Sethna, M. C. Kuntz, and O. Perković, *J. Magn. Magn. Mater.* **226**, 1287 (2001).
- [27] G. Bertotti and M. Pasquale, *J. Appl. Phys.* **67**, 5255 (1990).
- [28] S. Franz, G. Parisi, F. Ricci-Tersenghi, and T. Rizzo, *Eur. Phys. J. E* **34**, 102 (2011).
- [29] E. Vives and A. Planes, *Phys. Rev. B* **50**, 3839 (1994).
- [30] E. Vives and A. Planes, *J. Magn. Magn. Mater.* **221**, 164 (2000).
- [31] B. Alessandro, C. Beatrice, G. Bertotti, and A. Montorsi, *J. Appl. Phys.* **68**, 2901 (1990); **68**, 2908 (1990).
- [32] U. Schulz, J. Villain, E. Brézin, and H. Orland, *J. Stat. Phys.* **51**, 1 (1988).
- [33] B. Tadić, *Phys. Rev. Lett.* **77**, 3843 (1996).
- [34] I. Balog, G. Tarjus, and M. Tissier, *Phys. Rev. B* **97**, 094204 (2018).
- [35] J. P. Sethna, K. Dahmen, S. Kartha, J. A. Krumhansl, B. W. Roberts, and J. D. Shore, *Phys. Rev. Lett.* **70**, 3347 (1993).
- [36] E. Vives and A. Planes, *Phys. Rev. B* **63**, 134431 (2001).
- [37] N. G. Fytas and V. Martin-Mayor, *Phys. Rev. Lett.* **110**, 227201 (2013).
- [38] A. P. Young, *J. Phys. A: Math. Gen.* **10**, L257 (1977).
- [39] G. Parisi and N. Surlas, *Phys. Rev. Lett.* **43**, 744 (1979).
- [40] J. Bricmont and A. Kupiainen, *Phys. Rev. Lett.* **59**, 1829 (1987).
- [41] G. Parisi and N. Surlas, *Phys. Rev. Lett.* **89**, 257204 (2002).
- [42] M. Tissier and G. Tarjus, *Phys. Rev. Lett.* **107**, 041601 (2011).
- [43] N. G. Fytas, V. Martin-Mayor, M. Picco, and N. Surlas, *Phys. Rev. Lett.* **116**, 227201 (2016).
- [44] N. G. Fytas, V. Martin-Mayor, M. Picco, and N. Surlas, *Phys. Rev. E* **95**, 042117 (2017).
- [45] N. G. Fytas, V. Martin-Mayor, G. Parisi, M. Picco, and N. Surlas, *Phys. Rev. Lett.* **122**, 240603 (2019).
- [46] O. Perković, K. A. Dahmen, and J. P. Sethna, *arXiv:cond-mat/9609072* v1 (1996).
- [47] O. Perković, K. A. Dahmen, and J. P. Sethna, *Phys. Rev. B* **59**, 6106 (1999).
- [48] K. A. Dahmen and J. P. Sethna, *Phys. Rev. B* **53**, 14872 (1996).
- [49] F. J. Perez-Reche and E. Vives, *Phys. Rev. B* **67**, 134421 (2003).
- [50] F. J. Perez-Reche and E. Vives, *Phys. Rev. B* **70**, 214422 (2004).
- [51] Dj. Spasojević, S. Janičević, and M. Knežević, *Europhys. Lett.* **76**, 912 (2006).
- [52] Dj. Spasojević, S. Janičević, and M. Knežević, *Phys. Rev. Lett.* **106**, 175701 (2011).
- [53] Dj. Spasojević, S. Janičević, and M. Knežević, *Phys. Rev. E* **84**, 051119 (2011).
- [54] V. Navas-Portella and E. Vives, *Phys. Rev. E* **93**, 022129 (2016).
- [55] P. Shukla and D. Thongjaomayum, *J. Phys. A: Math. Theor.* **49**, 235001 (2016).
- [56] S. Janičević, S. Mijatović, and Dj. Spasojević, *Phys. Rev. E* **95**, 042131 (2017).
- [57] M. C. Kuntz, O. Perković, K. A. Dahmen, B. W. Roberts, and J. P. Sethna, *Comput. Sci. Eng.* **1**, 73 (1999).
- [58] Dj. Spasojević, S. Janičević, and M. Knežević, *Phys. Rev. E* **89**, 012118 (2014).
- [59] For example, let  $\{D_i(S_0), i = 1, \dots, n\}$  are the values of size distribution for avalanche size  $S_0$  found in  $i$ th of  $n$  simulations. Then the distribution value  $D(S_0)$  at  $S_0$  is the mean of this sample,  $D(S_0) = \frac{1}{n} \sum_{i=1}^n D_i(S_0)$ , and  $s_{D(S_0)} = s/\sqrt{n}$  is the standard error of that mean, where  $s$  is the sample standard deviation. The uncertainties, obtained in this way, are used (but, for simplicity, not plotted) in subsequent error estimation, e.g., in Monte Carlo estimation of the uncertainties of fitting parameters.
- [60] O. Perković, K. A. Dahmen, and J. P. Sethna, *Phys. Rev. Lett.* **75**, 4528 (1995).
- [61] M. Schwartz and A. Soffer, *Phys. Rev. Lett.* **55**, 2499 (1985).
- [62] N. G. Fytas and V. Martin-Mayor, *Phys. Rev. E* **93**, 063308 (2016).